Auto-generation in wall turbulence by the interaction of weak eddies

Goudar Vishwanathappa, M; Breugem, WP; Elsinga, GE

DOI
10.1063/1.4944048

Publication date
2016

Document Version
Final published version

Published in
Physics of Fluids

PHYSICS OF FLUIDS **28**, 035111 (2016)

Auto-generation in wall turbulence by the interaction of weak eddies

Manu V. Goudar,[a] W.-P. Breugem, and G. E. Elsinga
Laboratory of Aero and Hydrodynamics, Delft University of Technology, Delft 2628CA, The Netherlands

(Received 13 August 2015; accepted 1 March 2016; published online 21 March 2016)

For channel flow, we explore how commonly found weak eddies can still auto-generate and produce new eddies. Before, only strong eddies (above a threshold strength) were considered to auto-generate. Such strong eddies are rarely observed in actual turbulent flows however. Here, the evolution of two weak conditional eddies with different initial strengths, initial sizes, and initial stream-wise spacing between them is studied. The numerical procedure followed is similar to Zhou *et al*. ["Mechanisms for generating coherent packets of hairpin vortices in channel flow," J. Fluid Mech. **387**, 353 (1999)]. The two eddies are found to merge into a single stronger eddy when the initial upstream eddy is taller than the downstream eddy, which further auto-generates when the initial stream-wise separation is small (<120 wall units). However, it is observed that non-merging cases with small initial stream-wise separation also auto-generated. In the initial condition, the two conditional eddies are placed near to each other so their velocity fields (low-speed streaks and ejection events) get superimposed and amplified as a function of stream-wise spacing. To examine this effect, a divergence free low-speed streak is superimposed on an eddy. It is found that these low-speed streak simulations do not auto-generate. On the other hand, a rapid lift-up of an eddy by ejection events plays a role in the onset of auto-generation, which also leads to a modified interpretation of auto-generation mechanism. It differed from the existing auto-generation mechanism at the later stages of auto-generation where blockage of mean flow and shear layer deformation is considered instead of vortex dynamics.
[http://dx.doi.org/10.1063/1.4944048]

I. INTRODUCTION

In most engineering applications, we come across loss of energy/momentum in turbulent flows over solid surfaces, such as flow over a car or over the wings of an aircraft. It is desired to decrease this loss of energy when creating more efficient designs. For this, it is essential to understand the internal structure and detailed dynamics of wall-bounded turbulent flows. There are many different approaches to this problem. The approach that describes the turbulent flow in terms of so-called coherent structures will be considered in this paper.

One school of thought on the organized coherent structures is the hairpin eddy model in which the turbulent flow near a wall is populated by arch-type or hairpin-like vortices.[1] The initial generation of such hairpins in transitional boundary-layer flows has been studied by Brandt and de Lange.[2] In fully developed turbulent flows the hairpin vortices have been observed to be clustered into so-called hairpin packets,[3–5] which can be considered as a group of stream-wise aligned hairpin vortices, around a single low momentum region. The vortices within these packets are separated by 100-150 wall units[5,6] in the stream-wise direction. Due to their connection to the low momentum regions, hairpin packets are associated with turbulent kinetic energy, and as discussed by Adrian[1] and Ganapathisubramani, Longmire, and Marusic[7] they carry significant Reynolds shear stress.

[a]Electronic mail: m.goudarvishwanathappa@tudelft.nl

Moreover, conditional averaging around Reynolds shear stress event reveal hairpin packet kind of topologies[1,8] which again suggests hairpin type structures contribute importantly to the Reynolds shear stress. While other vortical structures may exist near the wall,[9,10] the close association of hairpin packets with the Reynolds shear stress makes them particularly relevant to the turbulent drag problem. It therefore becomes of interest to understand how packets come into existence.

The auto-generation mechanism[8] or parent-offspring concept[11] provides a possible explanation for this packet formation. In general, these mechanisms feature an initial eddy, which produces additional upstream eddies.[8,12] The detailed explanation on how a new eddy is generated has been subjected to debate.[8,11–15] Asai and Nishioka[14] conjectured the creation of new eddies is due to the inflectional instability of a wall shear layer lifted by the initial hairpin vortex legs. Their assessment was based on smoke-wire visualization and hot-wire measurements of boundary layer transition over a flat plate. On the other hand, Bake, Meyer, and Rist[15] argued vortex interactions are the main reason behind auto-generation rather than the shear layer after examining periodic Klebanoff transition on a flat plate experimentally and by a direct numerical simulation. The mechanism based on vortex dynamics was further elucidated by Zhou *et al.*[8] They came up with a simple model to demonstrate the auto-generation by numerical simulations of turbulent channel flow. Starting from a single, three dimensional vortex structure they studied its subsequent development. The initial vortex was the conditional eddy corresponding to the average velocity field around an ejection/Q2 event ($u' < 0,\ v' > 0$). The term eddy here refers to the vortex structure along with the velocity field around it. The subsequent dynamics were explained in terms of the induced motions of the vortex forming a kink in the legs of the initial hairpin which start to approach each other causing the associated shear layer to strengthen and roll-up into a span-wise vortex. The rolled-up span-wise vortex connects to the legs thereby creating the secondary vortex.

Zhou *et al.* also found that the conditional eddy only auto-generates new vortices upstream when its strength is above a certain threshold value. Kim, Sung, and Adrian[16] further demonstrated the robustness of this auto-generation mechanism by showing the generation of new vortices even in the presence of added noise, and a turbulent flow field. They also observed that the added background noise resulted in a reduction of the threshold strength required to trigger auto-generation, though mainly in the buffer layer. However, the conditional eddy that was introduced into the fully developed turbulent channel flow and finally resulted in auto-generation had very large values of velocities ($u',\ v'$) compared to the observed values in actual turbulent flows. The relative strength α which linearly amplifies the conditional eddy, and thereby the magnitude of the ejection event on which it is based, was found to be 6 in their case. The precise definition of α will be discussed in Sec. II. They increased α to get values of the swirling strength comparable with the actual turbulent flow eddies. However, our simulations indicate that $\alpha = 4$ already results in velocity values which are above the extreme values found in actual turbulent channel flow, as shown in Fig. 1. The probability of occurrence of velocity values at $\alpha = 3$ is even below 10^{-6} (see Fig. 1). The velocities corresponding to strength $\alpha = 2$ occur much less then the occurrence of velocities corresponding to $\alpha = 1$. The relative strength values of $\alpha = 2,\ 3$ were considered as the threshold strength for auto-generation in Zhou *et al.* On the contrary, in the present study values of $\alpha = 1$ are considered as

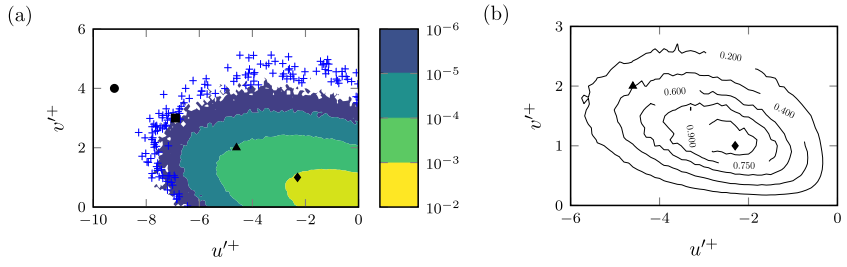

FIG. 1. (a) Normalized joint probability density function ($f_{u'v'}$) of u'^+ and v'^+ in the second quadrant at $y^+ = 51$. The scatter plot in the figure is used to show the extreme low occurrence events. (b) The contours of probability weighted Reynolds shear stress given by $-u'^+v'^+f_{u'v'}$ at $y^+ = 51$. Markers ♦, ▲, ■, and • in both figures correspond to relative strength $\alpha = 1,\ 2,\ 3,$ and 4, respectively.

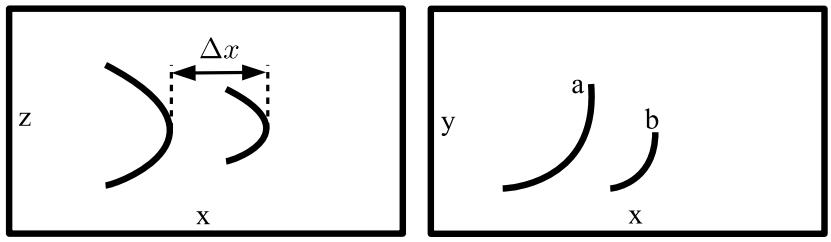

FIG. 2. Scenarios showing the arrangement of the two eddies in the initial condition. The left figure shows a top view and the right figure a side view of the channel. Δx is the stream-wise distance between the two vortices. In this example, the upstream vortex "a" is of higher event (y_e) location and the downstream vortex "b" is of lower y_e location.

it is of interest to consider scenarios involving weaker initial eddies, which are much more frequent in wall-bounded turbulence.

Therefore, in the first part of this study, we explore how a threshold strength eddy may come into existence by considering the interaction and possibly the merging of two weak initial eddy structures. By weak, we mean that the individual eddy is below the threshold strength and does not auto-generate by its own. Adrian, Meinhart, and Tomkins[5] suggested that different vortex packets can merge. The merging of entire clusters of vortices was also described by Lozano-Durán and Jiménez.[17] Merging of individual vortices was also observed in experiments.[18] Adrian, Balachandar, and Liu[19] showed the growth of span-wise scales by studying the span-wise merging, growth, and interaction of hairpin vortices. However, span-wise merging was reported to result in weaker, not stronger eddies. Therefore, it cannot be the origin of threshold strength eddies. Parthasarathy[20] studied multiple vortex interaction, however all the eddies under consideration were above threshold strength eddies. Based on these observations, the interactions between two ideal non-auto-generating eddies in the stream-wise direction are considered in this paper. The eddies are extracted from a fully developed channel flow simulation similar to Zhou *et al.*,[8] which will be discussed in detail in Sections II B and II C. A variety of scenarios are then created based on different initial strengths, different initial sizes, and different initial stream-wise spacings between the aligned eddies as shown in Fig. 2. The role of these quantities in the auto-generation mechanism is studied to understand their influence on the onset of auto-generation.

In the second part of this study, we investigate if low-speed streaks play a role in the onset of auto-generation. The low-speed streaks can affect auto-generation as they are sandwiched between the legs of the conditional eddy.[8] So, when two eddies are aligned behind each other as shown in Fig. 2, their low-speed streaks get superimposed and thereby strengthen (shown later in Fig. 4). In order to understand the effect of low-speed streaks in auto-generation, a divergence-free low-speed streak is added to a non-auto-generating conditional eddy and is studied for the generation of new eddies.

In the final part, critical aspects leading to the onset of auto-generation are identified and a modified interpretation of the auto-generation mechanism[8,14] is also presented. This interpretation for auto-generation is different from Zhou *et al.* at later stages of the development where it views shear layer deformation instead of vortex dynamics. Also, in Zhou *et al.*, a symmetric hairpin vortex with two legs was used to explain the auto-generation mechanism[8] which is not often found in actual turbulent flows.[10] Zhou *et al.* later added that the non-symmetric initial hairpins also auto-generated hairpin packets. These packets are more complicated but bear resemblance with the idealized symmetric case, showing long low-momentum zones and similar growth angles. Thus, the stages involving the mutual interaction and self-induction by the two legs, as in the model of Zhou *et al.*,[8] do not seem critically important. Hence, a stronger emphasis is laid on the role of the interaction of the hairpin with the background flow field.

II. METHODOLOGY

A. Numerical method

The dynamics of the eddies was simulated by Direct Numerical Simulation (DNS) in a channel flow driven by a constant pressure gradient. The pressure-correction method was used to solve

the Navier-Stokes equations, where the pressure distribution was only computed in the velocity corrector step in order to satisfy the constraint of a divergence free flow field (mass conservation). The explicit third-order Runge-Kutta scheme was employed for integration in time for advection and diffusion terms. And for spatial discretization, a pseudo-spectral (FFT-based)[21] method was used for the stream-wise (x) and span-wise (z) directions and a 6th order compact finite-difference scheme[22] for the wall-normal direction (y). Periodic boundary conditions were applied in the horizontal directions and no-slip, no-penetration conditions at the solid walls. The computational domain was fixed to $4\pi h \times 2h \times \frac{4}{3}\pi h$ in the x, y, and z directions with $192 \times 129 \times 128$ grid points, respectively. The uniform grid spacing was 11.78 and 5.89 wall units in the stream-wise and the span-wise direction, respectively. A non-uniform grid[23] was used in the wall-normal direction, where Δy^+ varied from 0.75 near the walls to 3.87 in the core of the channel. The superscript + refers to the scaling in viscous wall units. The velocities in the stream-wise, wall-normal, and span-wise directions are given by u, v, w or $u_i = u_1, u_2, u_3$ and the superscript $'$ on them represent perturbation velocities relative to the mean flow $U(y)$.

B. Conditional eddy

The initial condition at the start of a simulation is the superposition of the turbulent mean flow $U(y)$ and a perturbation velocity $\tilde{u}_i'$ associated with a conditional eddy. The turbulent mean flow was considered due to the high shear rate near the wall, which plays a role in the auto-generation.[1] The individual conditional eddy was extracted from a DNS of fully developed turbulent channel flow at $Re_\tau = 180$ by the means of linear stochastic estimation (LSE) of the flow field associated with an ejection event ($u' < 0$, $v' > 0$) identical to Zhou *et al.*[8] This initial condition was simulated by the DNS method introduced in Section II A. The pressure was not required to be initialized in the DNS, as the initial condition was a divergence-free flow field. The LSE approximates[24] the conditionally averaged flow field given by $\langle \mathbf{u}'(\mathbf{x}) | \mathbf{u}_\mathbf{e}'(\mathbf{x_e}) \rangle$ where $\mathbf{u}_\mathbf{e}'(\mathbf{x_e})$ represents the velocity event vector conditioned at point $\mathbf{x_e}$.

This LSE procedure has been extensively discussed in papers by Adrian[24,25] and is given by

$$\tilde{u_i}'(\mathbf{x}) = \text{Linear estimate of } \langle \mathbf{u}'(\mathbf{x}) | \mathbf{u}_\mathbf{e}'(\mathbf{x_e}) \rangle = \sum_{j=1}^{3} L_{ij}(\mathbf{x}, y_e) u_{j,e}', \quad i = 1,2,3, \tag{1}$$

where L_{ij} are linear estimate coefficients and $u_{j,e}'$ is the velocity event vector located at a wall-normal distance y_e. The coefficients L_{ij} are computed from unconditional two-point correlations according to

$$\sum_{j=1}^{3} \langle u_k'(\mathbf{x}_e) u_j'(\mathbf{x}_e) \rangle L_{ij} = \langle u_i'(\mathbf{x}) u_k'(\mathbf{x}_e) \rangle, \quad k = 1,2,3, \;\; i = 1,2,3, \tag{2}$$

where $\langle u_k' u_j' \rangle$ and $\langle u_i' u_k' \rangle$ represent the unconditional two-point co-variances between the velocities at $\mathbf{x}_e$, and between the fluctuating velocity field and the velocity at $\mathbf{x}_e$, respectively. In Equation (2), the correlations only depend on y_e, y, and the relative distances Δx, Δz with respect to the event as x, z are homogeneous directions in the flow. Hereafter the relative distances Δx and Δz will be simply represented as x and z, respectively, unless stated otherwise.

The velocity event vector $u_{j,e}'$ (see Eq. (1)) was chosen such that it matched to the value of the second quadrant (Q2) event ($u' < 0, v' > 0$) which contributes most to the Reynolds shear stress ($\langle u'v' \rangle$) at a particular wall-normal location (y_e^+). That is, the values of $u_e = u'$, $v_e = v'$ which maximizes $|u'v'| f_{uv}(u', v')$ in the second quadrant, where $f_{uv}(u', v')$ represents the joint probability density function of occurrence of u' and v'. The span-wise component w_e' was zero resulting in symmetric conditional eddy as shown in Fig. 3(a). The vortex is visualized by iso-surfaces of the square of local swirling strength[8] given by $\mathcal{S} = \lambda_{ci}^2$ which is used for vortex identification throughout this paper. The local swirling strength is defined as the imaginary part of a complex eigenvalue (λ_{ci}) of the velocity gradient tensor. If all the eigenvalues are real then the local swirling strength is zero. The values of the maximum swirling strength of the eddy conditioned at $y_e^+ = 51$ were found to be comparable with the reported values in Zhou *et al.*

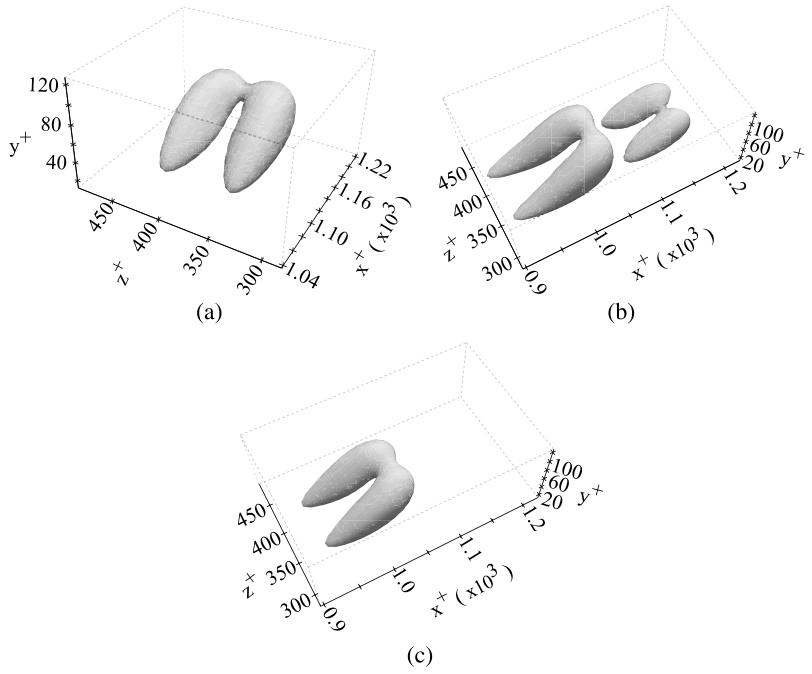

FIG. 3. Different initial conditions represented by the iso-surface of the square of local swirling strength $\mathcal{S}^+ = \lambda_{ci}^{+2} = 3.86 \times 10^{-4}$ (approximately 20% of maximum $\mathcal{S}^+$). (a) Single eddy case with event location ($y_e^+ = 76$) and relative strength of conditional eddy ($\alpha = 1$); (b) two vortex case, upstream vortex with ($y_e^+ = 76,\ \alpha = 1$) and downstream vortex ($y_e^+ = 51,\ \alpha = 1$); (c) low-speed streak superimposed (Eq. (4)) on vortex ($y_e^+ = 76,\ \alpha = 1$). It looks very similar to the single-eddy case ($y_e^+ = 76,\ \alpha = 1$).

C. Simulation types

Two of such conditional eddies were added to the turbulent mean flow $U(y)$ to study their interaction. The initial velocity field at the start of the simulation was given by

$$\tilde{u}_i(\mathbf{x}) = U(y) + \alpha \tilde{u}_i'(x, y, z; y_{e1}) + \beta \tilde{u}_i'(x + \Delta x, y, z; y_{e2}), \tag{3}$$

where α and $\tilde{u}_i'(x, y, z; y_{e1})$ are the relative strength and the perturbation velocity of the first eddy corresponding to the event at y_{e1}, and similarly the relative strength β, and perturbation velocities $\tilde{u}_i'(x + \Delta x, y, z; y_{e2})$ of the second eddy are based on the event at y_{e2} with an additional stream-wise shift (Δx) relative to the first eddy. The stream-wise shift is approximately the distance between the stream-wise locations of the maximum swirling strength of the eddies at time ($t^+ = 0$). Therefore Δx will be referred to as distance between two eddies throughout the paper. Figure 3(b) shows an example of an initial condition containing two eddies computed from Equation (3). An overview of all the two-eddy cases studied is given in Table I. Similar simulations[20] were performed previously, where the eddies considered were above the threshold strength and could auto-generate into new vortices individually. The values of the relative strength α, β listed in Table I correspond to cases where eddies do not auto-generate individually as it is aimed in the present paper to study below threshold strength eddies. The stream-wise spacing between the eddies (Δx) was chosen

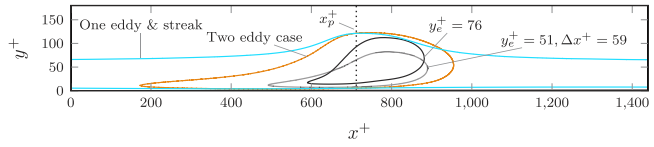

FIG. 4. Contours of low-speed streaks at $u'^+ = -1.0$. Black and green contours represent two individual eddies of relative strength $\alpha = 1$ at $y_e^+ = 76$ and 51. Two eddy case with eddies $(76, 51)$ and $\alpha = (1, 1)$ is given by red contour and blue contour corresponds to superposition of plane x_p^+ of $y_e^+ = 51$ on eddy $y_e^+ = 76$ as given in Eq. (4).

TABLE I. Overview of simulations of the cases with two eddies. "NA" or "not applicable" refers to cases where the initial vortices have already merged with each other. Case Ib and Ic, and case IIa and IIb are together as they have similar merging and auto-generation behavior for all Δx^+. Auto-generation is decided visually based on whether new eddies are generated when iso-surfaces at all time steps are drawn at 10% of the square of maximum initial swirling strength.

Case	Strength (α, β)	Ref plane (y^+_{e1}, y^+_{e2})	Spacing Δx^+	Merging	Auto-generation
Ia	(1,1)	(76, 51)	59	NA	Yes
			118	Yes	Yes
			177	Yes	Yes
			235	Yes	No
Ib		(103, 51)	59	NA	Yes
			118	Yes	No
Ic		(103, 76)	177	Yes	No
			235	Yes	No
IIa	(2,1)	(103, 51)	59	NA	Yes
			118	Yes	Yes
IIb		(103, 76)	177	Yes	Yes
			235	Yes	Yes
III	(1,1)	(76, 103)	59	NA	Yes
			118	No	Yes
			177	No	No
			235	No	No

comparable to the observed spacing of 100-140 wall-units in experiments[5,6,18] and below to study vortex-vortex interactions. Reference event planes (y_e) were considered in the outer layer and all event locations were between 0.1h to 0.3h in the wall normal direction. Case I and II simulations in Table I represent a taller upstream eddy compared to the downstream eddy and vice-versa in case III. In cases I and III both eddies have the same relative strength whereas the upstream eddy in case II eddy has a higher relative strength than the downstream eddy.

In the second part of this study, the interaction of a single conditional eddy with a low-speed streak is examined. To obtain the streak, the stream-wise velocity component in a cross-stream plane was extracted from the velocity field of a conditional eddy $\tilde{u}_i$ (Section II B). The extracted plane is at a stream-wise distance x_p relative to the event location $\mathbf{x}_e$. The streak is created by expanding this cross-stream plane uniformly in the x-direction. Hence the stream-wise derivative is zero. Furthermore, because $u_2 = u_3 = 0$, the streak is also divergence free and does not contain any vortex. Mathematically, the initial field containing one eddy and the streak is given by

$$\tilde{u}_i(\mathbf{x}) = U(y) + \alpha\tilde{u}'_i(x, y, z; y_{e1}) + \beta\tilde{u}'(y, z; y_{e2}, x_p), \tag{4}$$

where $\tilde{u}'(y, z; y_{e2}, x_p)$ corresponds to the stream-wise velocity at a plane x_p extracted from a conditional eddy conditioned to the event at y_{e2}, and β defines the relative strength of the streak as it linearly amplifies the velocities.

An overview of all the vortex-streak simulations is shown in Table II. Case IV is obtained by removal of the second, downstream eddy in the two eddy case Ia with $\Delta x^+ = 59$ (see Table I) and replacing it with a low-speed streak. This low-speed streak was obtained from the original downstream eddy in case Ia ($y^+_{e2} = 51$). It was the plane that overlapped with the peak swirling strength of the upstream eddy (i.e., $x^+_p = 59$). The streak is illustrated in Fig. 4. The contours of the low-speed streak for cases I, IV, and the single eddy cases of $y^+_e = 76$ and 51, as well as the plane x_p for case IV are shown in the figure. Case V is created to compare with the single eddy case of $y^+_e = 76$ with $\alpha = 2$. The low-speed streak was extracted from single eddy $y^+_e = 76$ with $\beta = 1$ at plane $x^+_p = 0$ and overlapped with the conditional eddy corresponding to the same event location and relative strength ($\alpha = 1$). The iso-surface of the square of swirling strength of this initial condition (case V)

TABLE II. Overview of simulations of the cases with a low-speed streak along with a eddy.

	Eddy		Low-speed streak		
Case	Event plane (y_e^+)	Strength (α)	Event plane (y_e^+)	Strength (β)	Spacing (x_p^+)
IV	76	1	51	1	59
V	76	1	76	1	0.0

is shown in Fig. 3(c). It is very similar to the single-eddy case of 76 with $\alpha = 1$ (Fig. 3(a)). However the strength of the low-speed streak is doubled. The two eddy case Ia with $\Delta x^+ = 59$, and the single eddy case of 76 with $\alpha = 2$ are the baseline cases, which are used to compare with the cases IV and V, respectively.

III. RESULTS AND DISCUSSION

A. Two eddy cases

The interaction between the two individually non-auto-generating eddies was studied to understand how above threshold strength eddies may come into existence. This was done by placing two non-auto-generating eddies behind each other aligned in stream-wise direction (see Section II C) and checking for auto-generation. Zhou *et al.*[8] described auto-generation as a means of generating new hairpin vortices from a parent hairpin vortex. In the present case, auto-generation is loosely referred to as the creation of new structures irrespective of whether these structures are hairpins or a pair of counter-rotating stream-wise vortices. An overview of the two-eddy cases studied is given in Table I. It is important to emphasize that all eddies shown in the table do not auto-generate individually, which was confirmed in separate simulations of the single eddies. Moreover, the single-eddy evolution was studied to set up a baseline for studying the interaction between two eddies. The initial conditional eddy is a pair of lifted, counter-rotating stream-wise vortices (Fig. 3(a)). Zhou *et al.*[8] report the following important observations connected with the evolution of a single eddy, which are confirmed by our simulations. All studied conditional eddies evolve into a hairpin vortex, which is referred to as the primary hairpin.[8] If it has sufficient initial strength, i.e., above a threshold strength, then it auto-generates. A conditional eddy with a higher swirling strength (or higher relative strength α) travels slower than a weaker eddy at the same event location (y_e^+). A conditional eddy based on an event specified at higher event vector location (y_e^+) travels faster for the same swirling strength due to higher mean flow velocity at larger wall normal location (y^+).[8]

Returning to the two eddy cases, Fig. 5 shows an example of two vortices merging to form a single vortex (Figs. 5(a) and 5(b)). This merged vortex subsequently auto-generates new vortices as shown in Fig. 5(c). As mentioned the two initial eddies do not auto-generate individually, i.e., they are all below the threshold strength required for auto-generation. Hence merging of *weak* eddies seems a viable concept to produce *stronger* eddies that do auto-generate. Table I lists the outcomes of the other two eddy simulations in terms of whether or not merging and auto-generation are observed. Two eddies separated by a stream-wise distance of $\Delta x^+ = 59$ were found to be merged already in the initial field for all the cases shown in Table I and hence merging is indicated in the table as not applicable (NA). Merging was observed for the cases I and II where the upstream eddy was at a higher event location compared to the downstream eddy. When the upstream eddy was at a lower event location compared to the downstream eddy, like in case III, merging did not occur. In cases I and II, the upstream eddy moved faster than the downstream eddy due to its higher location, reducing the distance between them with time and finally resulting in merging. From the single-eddy case, it was already known that an eddy with higher y_e^+ travels faster than an eddy with lower y_e^+ due to increasing mean flow velocity with y^+. After merging the geometric shape of

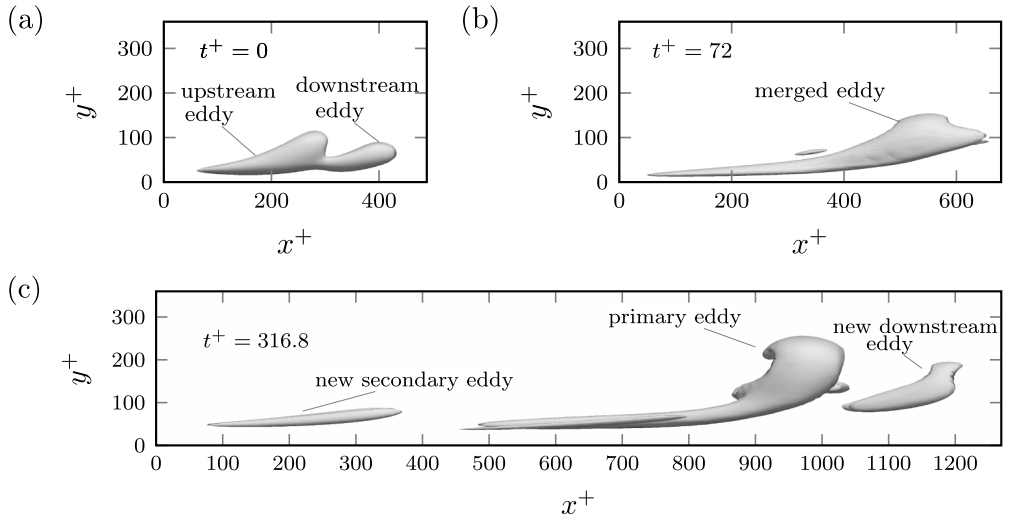

FIG. 5. Iso-contours of the swirling strength squared $\mathcal{S}^+ = 1.64 \times 10^{-4}$ (10% of maximum initial $\mathcal{S}^+$) at time $t^+ =$ 0, 72, and 316.8 for the two-eddy case Ia with $\Delta x^+ = 118$ (side view). At time $t^+ = 72$, the two initial eddies merge to create a single eddy. This merged eddy further auto-generates one upstream and one downstream vortex at $t^+ = 316.8$. In these plots x^+ is indicative of the size of the eddies rather than the distance travelled by them.

the structure remained broadly similar to a hairpin vortex. In case III, the downstream eddy travels faster and moves away from the upstream eddy hence they do not merge.

Auto-generation does not occur in all the simulations with vortex merging as indicated in Table I. Figures 5 and 6 represent examples of an auto-generation and a non-auto-generation case, respectively. In both simulations, the initial eddies were of unit strength ($\alpha = \beta = 1$) with the upstream eddy conditioned on $y_e^+ = 76$ and the downstream eddy on $y_e^+ = 51$ (case Ia, Table I). The only difference was in the stream-wise separation (Δx^+). For $\Delta x^+ = 118$, the two eddies (Fig. 5) merge after $t^+ = 72$ to form a single eddy. Then at time $t^+ = 316.8$, this merged eddy generates two new vortices, one upstream and one downstream as shown in Fig. 5(c). Merging is also observed for the larger stream-wise separation distance $\Delta x^+ = 235$ at $t^+ = 144$ (Fig. 6(a)). The development of this merged eddy at time $t^+ = 316.8$ can be seen in Fig. 6(b). It did not generate any new eddies and slowly dissipated with time. Similar cases where the auto-generation did not occur for large stream-wise separation can be found in Table I. This is because, as the separation distance increases, the time till merging increases as well. During this time, the strength of the eddies decay resulting in weaker eddies at the time of merging, hence a weaker interaction.

These interactions for different stream-wise spacing can also be quantified in terms of the vortex strength. The strength of the vortex at an instant in time is defined as the maximum of the swirling strength squared, which is normalized by means of its initial value (at $t^+ = 0$). The evolution of the two-eddy cases Ia with different stream-wise separations is shown in Fig. 7(a) along with the individual eddies at $y_e^+ = 76$ and 51 of strength $\alpha = 1$ for comparison. Similarly, Fig. 7(b) represents cases Ic along with individual eddies at $y_e^+ = 103$ and 76. In these figures, the square

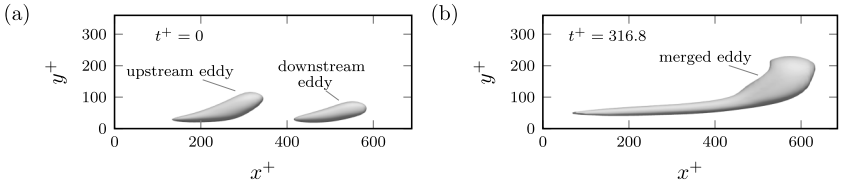

FIG. 6. Iso-contours of the swirling strength squared ($\mathcal{S}^+ = 1.64 \times 10^{-4}$) at time $t^+ = 0$ and 316.8 of the two-eddy case Ia with $\Delta x^+ = 235$. Similar to Fig. 5, two eddies merge but at a later time $t^+ = 144$. However the merged eddy does not auto-generate as observed in figure at $t^+ = 316.8$. In these plots x^+ is indicative of the size of the eddies rather than the distance travelled by them.

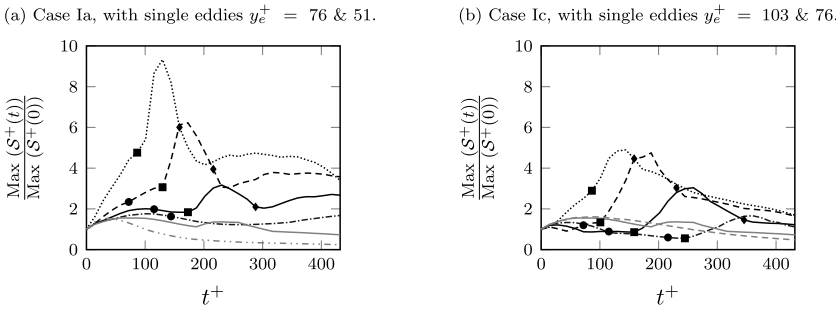

FIG. 7. Influence of stream-wise spacing on temporal evolution of normalized square of swirling strength: Dotted lines, dashed lines, solid lines, and dotted-dashed lines indicate stream-wise spacing $\Delta x^+ = 59, 118, 177,$ and 235, respectively. Gray dashed lines, gray solid line, and double dotted-dashed line represent individual eddies at event vector location 103, 76, and 51, respectively. Black filled square marker represents a shift in the peak location from the leg to the head, whereas black filled lozenge marker represents a shift from the head to the legs. Black filled bullet marker represents the time when merging is complete, which is visually decided (e.g., Fig. 5(b)).

of the initial maximum swirling strength ($\mathcal{S}^+(0)$) in two eddy and single eddy cases was found to be comparable to within 10% and therefore, it is used for normalization. The resulting normalized value represents the amplification of vortex strength compared to the initial state. At first the peak in swirling strength is located in the leg of the vortex then as the vortices merge and the hairpin shape develops, the peak location shifts to the hairpin head. This transition is indicated in Fig. 7 by the marker (■). After a while the swirling strength in the head starts to decrease and the peak in swirling strength returns to the legs, which is marked by (⧫) in Fig. 7. The marker (●) represents the time when merging is complete, which is visually decided (e.g., Fig. 5(b)).

In Fig. 7(a), it is observed that the initial growth rate (increase in vortex strength with respect to time) is much steeper for a stream-wise spacing of $\Delta x^+ = 59$ than for $\Delta x^+ = 118$. With increasing spacing the growth rate decreases and around $\Delta x^+ = 235$, it becomes similar to the single eddy cases. The peak amplification, i.e., the value of normalized maximum swirling strength squared, follows a similar trend. It reaches 9.33 for $\Delta x^+ = 59$ compared to 6.22 for $\Delta x^+ = 118$, and it continues to decrease as the stream-wise spacing is increased. The peak amplification of 9.33 in case Ia is about six times the value of 1.55 for the single eddy case with $y_e^+ = 76$. The two eddies thus temporarily produce a much stronger merged vortex (for $\Delta x^+ \leq 118$), which is above the threshold strength for auto-generation. Whereas individually, the eddies remain below the threshold strength and eventually get dissipated.[8] When the stream-wise distance between the eddies is higher, the time required to merge is longer, and during this time the eddies weaken individually. And when these weak eddies merge, the merged eddy is not strong enough to generate new vortices. Similar observations can be made in Fig. 7(b), where again the peak amplification decreases as the stream-wise spacing is increased.

The peak amplification is also found to increase when the distance between the two eddies in the wall-normal direction is decreased. The upstream eddy for both cases Ib and Ic is conditioned at $y_e^+ = 103$ however the downstream eddy was conditioned at $y_e^+ = 51$ for case Ib and $y_e^+ = 76$ for Ic. The peak amplification in case Ic was found to be 4.89 (see Fig. 7(b)) compared to 3.14 for case Ib with stream-wise spacing $\Delta x^+ = 59$. A similar trend of higher peak amplification was observed in case IIb compared to IIa where the downstream eddy in case IIa was conditioned at lower y^+ than case IIb.

In cases IIa and IIb (Table I), where the stream-wise spacing was higher ($\Delta x^+ = 235$) the merged eddy did auto-generate even though the stream-wise spacing between the two eddies was large for vortex-vortex interaction. This was due to the higher initial strength of the eddy, though it was still below threshold strength.

From all these observations, it can be inferred that stream-wise merging results in the creation of a stronger vortex whose subsequent auto-generation may still depend upon the initial strength of eddies and their stream-wise spacing. The strength of the initial eddies (α and β) required for auto-generation in the cases I was around unity, which corresponds to an eddy conditioned on a

commonly occurring ejection event. This is clearly lower than the threshold strength of a single eddy required for auto-generation.[8] However, auto-generation was also observed in cases where merging did not occur (see case III, Table I). This clearly indicates that vortex merging is not the only mechanism that can trigger auto-generation. It was also found that the auto-generation occurred in non-merging cases only when the stream-wise spacing was lower than 118 wall units. From these observations, it can be educed that the stream-wise separation (Δx^+) between eddies plays a major role in auto-generation. However, the initial stream-wise separation cannot be identified as the sole parameter to define the onset of auto-generation, as auto-generation also depends upon the strength of the eddies in our simulations. The initial strength α was used as a quantity to define the onset of auto-generation in Zhou *et al.*[8] However, in the present investigation below threshold strength eddies were considered and still new structures were generated when the stream-wise spacing was sufficiently small. This may be because when two eddies are placed near to each other their fluctuating velocity fields get superimposed onto each other and amplified, which is similar to an increase in threshold strength where the velocity field is linearly amplified. The magnitude of the superimposed fluctuating velocity at a given spatial location decreases with the increase in stream-wise separation between the two eddies (see Fig. 4). So, threshold strength and stream-wise spacing (Δx^+) are both related to the velocity field. A quantity defining the velocity field, like ejection events or low-speed streaks, may thus be used to define the onset of auto-generation.

B. Role of low-speed streaks

An extracted conditional eddy consists of a vortex on top of a low speed streak. So when two conditional eddies are superimposed, their low-speed streaks are also superimposed. In order to separate the effect of overlapping low-speed streaks, an extracted low-speed streak is superimposed under a conditional eddy and simulated to check for the generation of new vortices. In order to create a low speed streak, the vortex was removed from a conditional eddy as described in Section II C. The streak was then added to a conditional eddy as shown in Equation (4). An overview of the simulations is given in Table II. Case IV nor Case V revealed any signs of auto-generation. Figure 8 represents the temporal evolution of the normalized maximum swirling strength of cases IV and V along with the baseline cases where auto-generation occurs. It was observed that adding a low-speed streak did not cause an increase or amplification of the maximum normalized $\mathcal{S}^+$ in contrast to the baseline cases which included vortical structure in the second eddy. From this, it is inferred that the overlapping of the low-speed regions (in the two eddy cases) is not the main cause of the subsequent auto-generation.

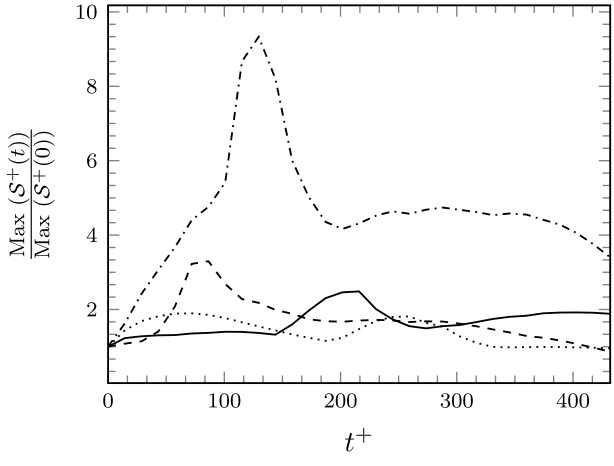

FIG. 8. Temporal evolution of normalized maximum swirling strength. Lines (⋯) and (-·-) refer to case IV and its baseline simulation (case I (76,51), $\Delta x^+ = 59$). Lines (—) and (---) refer to case V and its baseline simulation (single eddy $y_e^+ = 76$ and $\alpha = 2$).

From the above, we infer that vortex-streak interactions do not explain auto-generation, hence cannot be used to predict the onset of auto-generation. As ejection events are used to extract the conditional eddy, their role in the auto-generation mechanism is studied in a more detailed way in Subsection III C.

C. A modified interpretation of the auto-generation mechanism

The auto-generation mechanism proposed by Zhou *et al*. is based on vortex dynamics where self- and mutual induction play an important role. In the following we propose a modified description of auto-generation especially concerning the onset of the formation of the secondary hairpin vortex. We will not only consider vortex induction but also put a stronger emphasis on the environment of the primary hairpin. After all, the initial eddy does not only contain a hairpin vortex but also the imprint of its surrounding structures that are statistically important. The modified interpretation of creating new eddies utilizes the ideas of shear-layer instabilities conjectured by Asai and Nishioka.[14] In the following paragraphs, this will be discussed in detail.

Figure 9 illustrates the evolution of the two eddy case Ia with the stream-wise separation of $\Delta x^+ = 59$. The vectors in the plot are scaled to unit length, hence only indicating the flow direction. This aids in better visualization of the shear layer roll-up. Figures 9(a)–9(e) were plotted for time $t^+ = 28.8$, 57.6, 86.4, 158.4, and 244.8, respectively.

The initial development can be explained from Figure 9(a). The vortex is contained within a low speed region, which is clearly larger and taller than the vortex itself.[5,26] This large size region can play a role in the auto-generation mechanism, and is not explained by induction of a single hairpin. Assuming the initial stages of development as largely passive, meaning advection of the vortex is by the local velocity, it is seen from Fig. 9(a) that the wall-normal velocity is large in point "A2," i.e., the head as compared to point "A1" in the legs. Consequently, the head lifts away from the wall faster than the legs, which is indeed observed (Figs. 9(c)–9(e)). At the same time, the stream-wise velocity ($U + u'$) in "A2" is higher compared to "A1," which means the legs are stretched (Figs. 9(b)–9(e)). The combination of these two effects is observed in Figs. 9(b)–9(e), where the angle of the legs near the head and the shear layer just upstream of the head grows steeper.

In Fig. 9(a), a shear layer upstream of the initial hairpin vortex is visible at an angle with respect to the wall.[5] This occurs when the ejected fluid between the legs meets the incoming (high velocity) flow. After 28.8 wall time units, i.e., at $t^+ = 57.6$ (Fig. 9(b)), as the velocity at the location

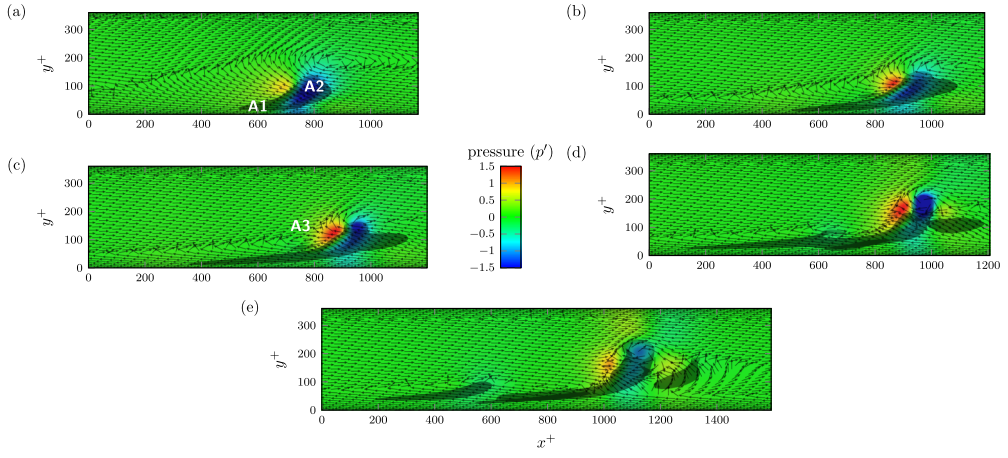

FIG. 9. Auto-generation mechanism : Vector plots of velocity (u'^+, v'^+) along with fluctuation pressure (p') contours in the symmetry plane which is between the two legs of an eddy. All vector are scaled by unit length, hence only indicate the flow direction. The iso-surfaces in the figures correspond the 10% of the initial maximum swirling strength. This is for two eddy case (76,51) at strength $\alpha = (1, 1)$ with $\Delta x^+ = 59$. (a)–(e) represent the evolution of two eddies and vector plots in time (t^+) 28.8, 57.6, 86.4, 158.4, and 244.8, respectively.

of the head is higher than the un-lifted part due to its higher y^+, the legs get stretched in the stream-wise direction and amplify (see Fig. 7). At the same time, the head of the vortex moves up in the wall-normal direction as discussed above and the swirling strength of the head increases. This increase in strength appears to be associated with the hairpin head approaching the shear layer where the velocity differences across the layer strengthen the roll-up (see Fig. 7). The stronger roll-up increases the vortex induced flow leading to a stronger ejection of the fluid between the legs near the head and a stronger self-induction[8] which lifts the head even further from the wall. Furthermore, the angle of the shear layer and the lifted stream-wise legs become steeper. With time, the hairpin head is lifted above the initial shear layer and starts to obstruct the incoming high velocity flow. This is indicated by high pressure region upstream of the head in Figs. 9(c) and 9(d). Due to the blockage, a stagnation point in (u',v') is formed within the now heavily distorted shear layer upstream of the lifted primary hairpin. The stagnation point is associated with a local pressure peak which deflects incoming flow away from the hairpin head resulting in a local saddle point topology (labeled "A3" in Fig. 9(c)). Most of the incoming flow is deflected up and over the primary hairpin head, but some fluid is pushed downward. This downward flow interacts with the low speed flow underneath causing a roll-up of the shear-layer,[14] which marks the birth of the secondary hairpin head Fig. 9(c). The secondary hairpin head is observed to distort the legs and create a kink in them. The un-lifted legs just upstream of the primary hairpin head are pushed down as shown in Fig. 9(d). This sequence is different from the interpretation given by Zhou *et al.* where the kinks in the legs develop *before* the new hairpin head is created. With time, as the new roll-up gets stronger, the upstream un-lifted legs of the stream-wise vortex gets attached to it. This attachment of head to the legs is a viscous process.[8]

The stronger ejection with time lifts up the new secondary hairpin similar to the description of the points "A1" and "A2" in Fig. 9(a). This causes the stream-wise vortex to lift up at the point of the new hairpin and the sweep events downstream of the new head push the stream-wise legs down towards the wall. This leads to the separation of the new vortex from the original stream-wise vortex (Fig. 9(e)). If the ejection events in the new leg are stronger than a third vortex is formed in a similar way or else it gets dissipated with time. A third vortex formation has also been observed between the old and the new vortices when the ejection in the leg of the old vortex is strong.

From the above observations, the auto-generation is summarized as the rapid lift up of a hairpin vortex which blocks the incoming flow leading to the roll-up of the shear layer creating a secondary vortex. The rapid lift up of the initial hairpin is identified to be critical element in the onset of auto-generation. In the present simulations, the rapid lift up is observed in three scenarios, (i) a single beyond threshold strength eddy, (ii) merging eddies, and (iii) non-merging cases of below threshold strength eddies. In the first scenario, as the strength of a hairpin vortex is increased, its environment, i.e., ejection events become stronger. This along with the self-induction leads to the rapid lift up of the hairpin vortex. In the second scenario (Case I and II), two weak hairpin vortices merged to form a stronger hairpin. Also the ejection events at the beginning of simulation were stronger due to the superposition of two vortices. The creation of a stronger vortex along with the enhanced ejection events leads to the faster lift up of a merged eddy. In the last scenario of the non-merging case of week eddies (case III), when the stream-wise spacing between eddies was sufficiently small, the ejection of fluid by the downstream eddy propelled the upstream eddy away from the wall. Also, similar to the merging case, the superposition of two eddies leads to the creation of a stronger ejection event. The combined effect lifts the upstream eddy away from the wall. So ejection events play a critical role in the rapid lift up of the vortex, which then interacts with the incoming flow to create a new hairpin.

In this new modified interpretation, two stream-wise vortices are not required to describe the lift up and further auto-generation as is the case in Zhou *et al.* A single leg can lift up and block the incoming flow leading to shear layer roll up and creation of a new vortex. This is one of the advantages of the present interpretation as it does not rely on the presence of two stream-wise vortex legs which are not often found in actual turbulent flows.[10] It also further strengthens the existing hairpin eddy model.[5]

IV. CONCLUSIONS

We explored how an above-threshold strength eddy may come into existence, the role of a low-speed streak in the onset of auto-generation and also proposed a modified interpretation of the auto-generation mechanism. This was done by performing a series of direct numerical simulations of turbulent channel flow at $Re_\tau = 180$ with idealized initial conditions. The initial condition was the sum of the mean velocity profile at $Re_\tau = 180$ and the perturbation velocity corresponding to a conditional eddy extracted by LSE from fully developed turbulent channel flow data at the same Reynolds number.

The two conditional eddies which do not auto-generate individually were aligned behind each other in the stream-wise direction to study the interactions that lead to auto-generation. It was found that two eddies merged when an eddy conditioned at higher wall-normal location was placed upstream of the one conditioned at the lower wall-normal location. The eddy with higher wall-normal location moved faster due to higher mean velocity and merged with the downstream eddy. The maximum normalized square of swirling strength increased after merging. Hence, merging can lead to the creation of above threshold strength eddy. However all the merging cases did not auto-generate, only the cases with lower stream-wise separation auto-generated. As the initial distance between the eddies increased, merging took longer time, during which the eddies weakened individually and hence the merged eddy was not strong enough to create new vortices. However, when the initial strength of the eddies was increased the merged eddy auto-generated even for larger stream-wise separations. From these observations, it is inferred that merging can create stronger eddies but subsequent auto-generation may still depend upon initial strength or the initial stream-wise separation.

For small initial stream-wise separations, a few non-merging eddy cases also generated new structures. Merging was not possible in these cases as the downstream eddy convected faster than the upstream eddy as it was conditioned at a higher wall-normal location compared to the upstream eddy. Hence, merging is not the only mechanism to trigger auto-generation. The small stream-wise separation is identified as a quantity to play a role in the onset of auto-generation.

Zhou *et al*. used threshold strength in the initial condition to define the onset of auto-generation in single eddy cases. In present case, where the two eddies were below threshold strength, auto-generation was found to depend largely on the stream-wise separation. The smaller stream-wise separation between eddies emulate increasing threshold strength as velocity fields in both cases got amplified. Hence, the role of the velocity field and specifically of the low-speed streak was explored for the onset of auto-generation. When the stream-wise separation was smaller, low-speed streaks from the two eddies got superimposed and amplified. A separate set of simulations were performed by adding a divergence-free low-speed streak to a conditional eddy to understand the influence of vortex-streak interactions on the auto-generation. These simulations did not result in any auto-generation or amplification of the normalized maximum swirling strength compared to the baseline cases (Fig. 8).

At the end, a modified interpretation of the auto-generation mechanism based on the ejection events and its interaction with surrounding flow is presented. Inspection of the data suggests that a strong lift-up of hairpin head by the ejection event coupled with a stream-wise vortex can lead to auto-generation as shown in Fig. 10. A stream-wise vortex with a small span-wise swirl, i.e., head (Fig. 10(a)), is rapidly lifted up by the ejection events. Due to the lift up of the vortex head, the in-rushing flow is blocked (Fig. 10(b)). This inrush of flow and the already existing ejection events cause the shear layer to deform and roll-up in the span-wise direction just upstream of the vortex (Figs. 10(c) and 10(d)). As this span-wise roll-up becomes stronger, it connects to the leg/legs of the downstream vortex. With time, this becomes a new vortex and gets separated from the main vortex (Figs. 10(d) and 10(e)). If the ejection events are stronger in any of the two vortices, a third eddy will be formed in a similar way, else the eddies are dissipated over time. The generation of new vortices was also observed in experiments by Jodai and Elsinga[27] within a fully turbulent boundary layer in a similar way.

This modified mechanism differs from the existing mechanism by Zhou *et al*. where induced vortex motions result in formation of a kink in the legs of the initial eddy (Fig. 10(d)) before a

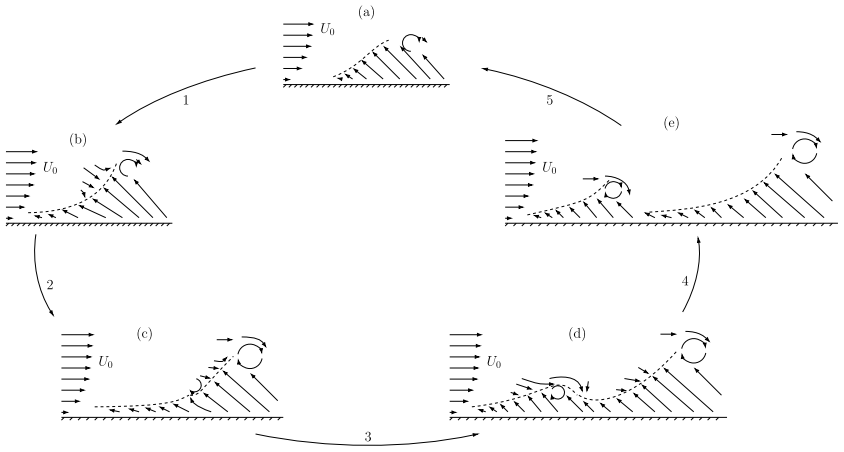

FIG. 10. Two-dimensional schematic of auto-generation mechanism shown in Fig. 9. Vectors indicate (u', v'), - - - - represents the shear-layer and U_0 indicates the mean flow. (a) Initial hairpin with a shear-layer. (b) Head of the hairpin lifts up rapidly blocking the incoming flow. Formation of a stagnation/saddle point forces fluid to move towards head or towards wall. (c) Fluid moving towards the wall deforms the shear-layer and initiates the shear-layer roll up. (d) Continued lift up of the initial hairpin head deforms the shear-layer further. At the same time, as the new roll-up strengthens, the fluid downstream is pushed down and the Q2 event upstream of the roll-up is enhanced. (e) The new hairpin vortex detaches form the original hairpin.

new hairpin head is created. In other words, kink formation in Zhou *et al*. is due to the mutual and self-induction of the stream-wise legs, whereas in the present mechanism it is the consequence of shear layer roll-up and ejection events. Also, the presence of two stream-wise vortex legs is not necessary to describe the onset of auto-generation as a single leg can lift up and block the incoming flow leading to the shear-layer roll up and further generating a new eddy.

The implication of the present study is that commonly found weak eddies can also auto-generate, which further strengthens the existing hairpin eddy model.[1]

ACKNOWLEDGMENTS

The authors kindly thank Professor B. J. Boersma and Dr. ir. M. J. B. M. Pourquie for suggestions and help in the usage of the supercomputer and Professor B. J. Boersma for valuable inputs on creating a DNS code. The authors also thank the Dutch Technology Foundation STW for their financial support.

[1] R. J. Adrian, "Hairpin vortex organization in wall turbulence," Phys. Fluids **19**, 041301 (2007).
[2] L. Brandt and H. C. de Lange, "Streak interactions and breakdown in boundary layer flows," Phys. Fluids **20**, 024107 (2008).
[3] M. R. Head and P. Bandyopadhyay, "New aspects of turbulent boundary-layer structure," J. Fluid Mech. **107**, 297–338 (1981).
[4] C. R. Smith, "A synthesized model of the near-wall behavior in turbulent boundary layers," in *Proceedings of the 8th Symposium of Turbulence*, edited by J. L. Zakin and G. Patterson (University of Missouri-Rolla, Rolla, 1984).
[5] R. J. Adrian, C. D. Meinhart, and C. D. Tomkins, "Vortex organization in the outer region of the turbulent boundary layer," J. Fluid Mech. **422**, 1–54 (2000).
[6] M. S. Acarlar and C. R. Smith, "A study of hairpin vortices in a laminar boundary layer. Part 2. Hairpin vortices generated by fluid injection," J. Fluid Mech. **175**, 43–83 (1987).
[7] B. Ganapathisubramani, E. K. Longmire, and I. Marusic, "Characteristics of vortex packets in turbulent boundary layers," J. Fluid Mech. **478**, 35–46 (2003).
[8] J. Zhou, R. J. Adrian, S. Balachandar, and T. M. Kendall, "Mechanisms for generating coherent packets of hairpin vortices in channel flow," J. Fluid Mech. **387**, 353–396 (1999).
[9] S. K. Robinson, "Coherent motions in the turbulent boundary layer," Ann. Rev. Fluid Mech. **23**, 601–639 (1991).
[10] P. Schlatter, Q. Li, R. Örlü, F. Hussain, and D. S. Henningson, "On the near-wall vortical structures at moderate Reynolds numbers," Eur. J. Mech., B: Fluids **48**, 75–93 (2014).
[11] C. R. Smith, J. D. A. Walker, A. H. Haidari, and U. Sobrun, "On the dynamics of near wall turbulence," Philos. Trans.: Phys. Sci. Eng. **336**, 131–175 (1991).
[12] A. H. Haidari and C. R. Smith, "The generation and regeneration of single hairpin vortices," J. Fluid Mech. **277**, 135–162 (1994).
[13] B. A. Singer and R. D. Joslin, "Metamorphosis of a hairpin vortex into a young turbulent spot," Phys. Fluids **6**, 3724–3736 (1994).

[14] M. Asai and M. Nishioka, "Boundary-layer transition triggered by hairpin eddies at subcritical Reynolds numbers," J. Fluid Mech. **297**, 101–122 (1995).
[15] S. Bake, D. G. W. Meyer, and U. Rist, "Turbulence mechanism in Klebanoff transition: A quantitative comparison of experiment and direct numerical simulation," J. Fluid Mech. **459**, 217–243 (2002).
[16] K. Kim, H. J. Sung, and R. J. Adrian, "Effects of background noise on generating coherent packets of hairpin vortices," Phys. Fluids **20**, 105107 (2008).
[17] A. Lozano-Durán and J. Jiménez, "Time-resolved evolution of coherent structures in turbulent channels: Characterization of eddies and cascades," J. Fluid Mech. **759**, 432–471 (2014).
[18] G. E. Elsinga, C. Poelma, A. Schröder, R. Geisler, F. Scarano, and J. Westerweel, "Tracking of vortices in a turbulent boundary layer," J. Fluid Mech. **697**, 273–295 (2012).
[19] R. J. Adrian, S. Balachandar, and Z. C. Liu, "Spanwise growth of vortex structure in wall turbulence," KSME Int. J. **15**, 1741–1749 (2001).
[20] P. K. Parthasarathy, "Dynamics of vortices in numerically simulated turbulent channel flow," M.S. thesis, Arizona State University, 2011.
[21] M. Frigo and S. G. Johnson, "The design and implementation of FFTW3," Proc. IEEE **93**, 216–231 (2005), special issue on "program generation, optimization, and platform adaptation."
[22] B. J. Boersma, "A 6th order staggered compact finite difference method for the incompressible Navier-Stokes and scalar transport equations," J. Comput. Phys. **230**, 4940–4954 (2011).
[23] B. J. Boersma, "A staggered compact finite difference formulation for the compressible Navier-Stokes equations," J. Comput. Phys. **208**, 675–690 (2005).
[24] R. J. Adrian, "Stochastic estimation of the structure of turbulent fields," in *Eddy Structure Identification*, CISM International Centre for Mechanical Sciences Vol. 353, edited by J. P. Bonnet (Springer-Verlag, 1996), pp. 145–196.
[25] R. J. Adrian, "Stochastic estimation of conditional structure: A review," Appl. Sci. Res. **53**, 291–303 (1994).
[26] G. E. Elsinga, R. J. Adrian, B. W. Van Oudheusden, and F. Scarano, "Three-dimensional vortex organization in a high-Reynolds-number supersonic turbulent boundary layer," J. Fluid Mech. **644**, 35–60 (2010).
[27] Y. Jodai and G. E. Elsinga, "Experimental observation of hairpin auto-generation events in a turbulent boundary layer," J. Fluid Mech. (to be published).